Supporting Information

A. The relationship between L_x and L_y and throughput increase.

The throughput increase is a metric that describes how much of the final pattern consists of PDMS microdomains vs. posts made by electron beam lithography (EBL), *i.e.* the factor by which the block copolymer self-assembly can be considered to enhance the throughput of an EBL system, compared to writing the entire pattern using EBL. It is defined as the area of the final PDMS pattern divided by the area of the HSQ posts that were written. The throughput increase is proportional to L_x and L_y of the post array, i.e. inversely proportional to the density of the posts. As the post spacing increases it becomes more likely that multiple in-plane orientations of the cylinders will form because the difference in strain energy between competing orientations decreases.[1] This leads to formation of defects in the templated microdomain arrays, and limits the throughput increase which can be achieved by topographic templates. In Figure 1, throughput increases of the order of 20 were demonstrated with the presence of a few defects per square μm under the annealing conditions used.

B. Dashes can be used to increase the throughput over 66-fold.

In the case when L_x was larger than 72 nm, only a fraction of cylinders aligned along the *y*-axis, which was the commensurate orientation for L_x of 72 nm. To prevent the cylinders from being oriented in unwanted orientations, a template consisting of an array of dashes (line segments) was used instead of posts. L_y of the array was fixed at 100 nm, and the length of the dashes was fixed at 60 nm.

When L_x was 18 nm, an array of dashes acted as trenches rather than topographic templates. As figure S1 shows, the cylinders aligned along the *x*-axis. When L_x was larger than 20 nm, the arrays acted as topographic templates and guided the cylinders along the *y*-axis. For dash-arrays with L_x of 708 nm, only 1/66 of the final pattern was fabricated by EBL.

To estimate the templating effect of the dash-arrays, the area fraction of the cylinders which made an angle between 80 ^{o} and 90 ^{o} with the *x*-axis was calculated by using an image-analysis program. If all angles between 0 ^{o} and 90 ^{o} were equally probable, the area fraction of cylinders oriented along an angle between 80 ^{o} and 90 ^{o} would be around 11.1 %. As shown in figure S1, the area fractions of cylinders oriented along the *y*-axis were higher than 50 % for dash-arrays with a range of L_x of 85 nm to 756 nm. At some specific L_x, the area fractions reached 90 %. To estimate how the commensurate conditions are applied to the dash-arrays, the deviation of L_x from the commensurate condition for an orientation parallel to the *y*-axis was calculated. The commensurate condition for the orientation parallel to the *y*-axis is an integer multiple of the equilibrium period L_o (=~~18~~ 18 nm). As shown in figure S1(f), the area fractions of the cylinders oriented along the *y*-axis decreased as L_x deviated from commensurability. This result implies that the *y*-axis orientation competes with other orientations when the L_x does not satisfy the commensurate condition for orientation parallel to the *y*-axis. Dash-arrays can increase the area fraction of the orientation parallel to the *y*-axis up to 90 % when L_x satisfies the commensurate condition.

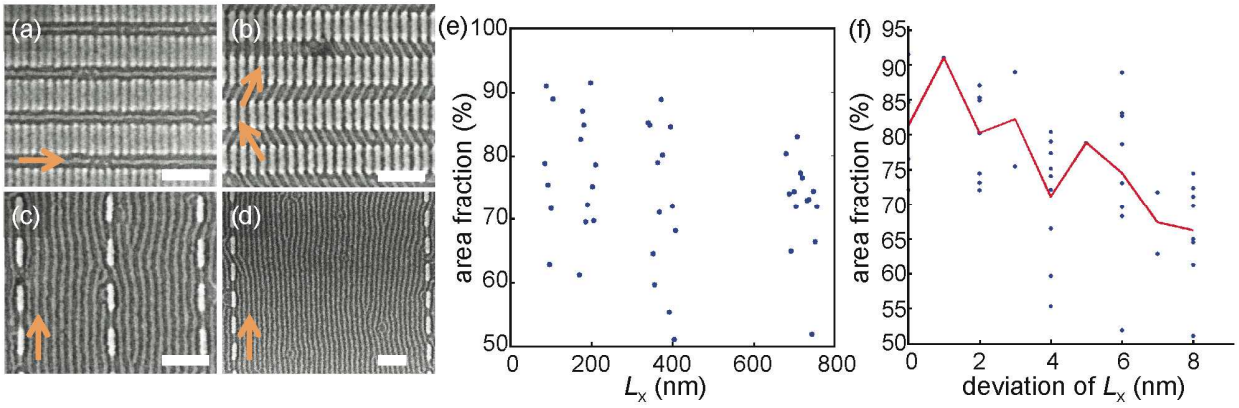

Figure S1. Block copolymers templated by dash-arrays. (a~d) Scanning electron micrograph images of PDMS microdomains templated by dash-arrays with various L_x. L_y was fixed at 100 nm and the length of each dash was fixed at 60 nm. L_x was (a) 18 nm (b) 21 nm (c) 198 nm (d) 708 nm. Scale bar = 100 nm. (e) Plot of the area fraction of PDMS oriented along the *y*-axis vs. the pitch of dashes. The area fraction was calculated by using an image-analysis program written in MATLAB. (f) Plot of the area fraction of PDMS cylinders oriented along the *y*-axis vs. the deviation of L_x from the commensurate condition for the orientation parallel to the *y*-axis. The commensurate condition for the orientation parallel to the *y*-axis is an integer multiple of the equilibrium periodicity L_o (18 nm).

C. The area fraction distributions of the PDMS cylinders.

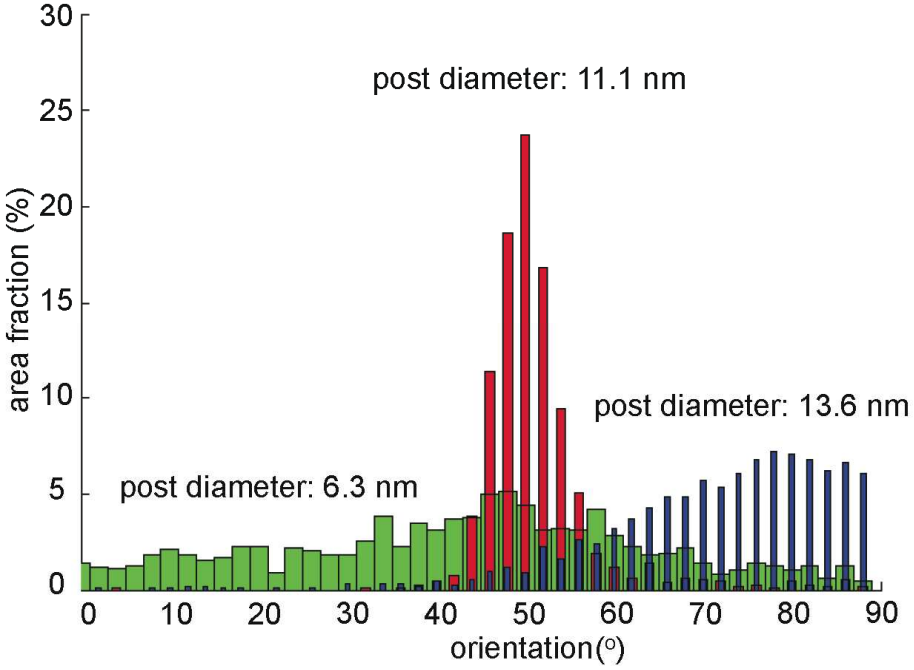

Figure S2. The area fraction distributions of the PDMS cylinders templated by posts with a height of 16 nm and a range of diameters as a function of in-plane orientation. The width of bars were adjusted to make all three area fraction distributions visible on the same axes. Post diameter is (green bars) 6.3 nm, (red bars) 11.1 nm, and (blue bars) 13.6 nm. Due to the distortion of the PDMS cylinders around the posts, the orientation of the PDMS cylinders can be measured with a few degrees error.

Figure S2 shows the area fraction distributions for PDMS cylinders as a function of the in plane orientation of the cylinders. The area fraction of the PDMS cylinders templated by posts with a diameter of 6.3 nm (green bars) is uniform over all the orientations, which means the PDMS cylinders were not aligned in a preferential orientation. This implies that posts with a diameter of 6.3 nm did not template the self-assembly of 16 kg/mol PS-*b*-PDMS. PDMS

cylinders templated by posts with a diameter of 11.1 nm (red bars), which is similar to the diameter of the PDMS microdomains, were aligned in the commensurate orientation. However, PDMS cylinders oriented parallel to the *y*-axis when templated by posts with a diameter of 13.6 nm (blue bars).

D. SCFT simulation parameters.

The SCFT simulations used to model the system uses the same formulation of the theory as presented in the supporting information section of Mickiewicz *et. al*.[2] For the systems considered, the SCFT calculations were carried out on a 24x16x20 grid, volume fraction of the minority component f = 0.33, number of statistical segments in the chain used was 69 modeling the approximate number of Kuhn monomers in the real PS-b-PDMS system, and a χN = 14.0 modeling the reduced Flory-Huggins solubility parameter encountered in the solvent annealing. The cell dimensions were chosen to correspond to the real dimensions of a 48 nm by 32 nm post spacing with the thickness being selected as an intermediate thickness encountered during the solvent annealing. The natural polymer period L_o corresponds to 9 grid points in the simulation grid. The simulations were run for 300,000 iterations to ensure the energy of the system was unchanging thus corresponding to an energy minimum structure. The posts, air interface, and polymer brush layer were all modeled by constraining the fields to take on set values at the locations corresponding to those features with a large potential barrier to both the majority and minority block for the posts and substrate and an attractive potential to the minority block for the air interface and brush layer. A schematic showing these boundary conditions is shown in Figure S3. In addition to the topographical, chemical, and surface boundary conditions, the simulations

used periodic boundary conditions in the *x* and *y* directions, thus having the system are a unit cell in an infinitely periodic lattice.

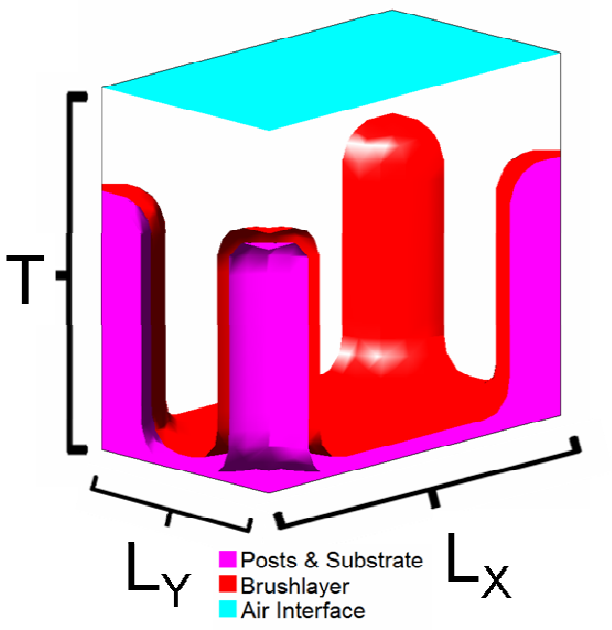

Figure S3. Schematic diagram showing the boundary conditions implemented in the SCFT simulations. The purple region represents the area where the fields were constrained to be a high potential barrier to both blocks of the polymer to model the posts and substrate, the red region represents the area were the fields were constrained to be attractive to the minority component to model the polymer brush layer, and the blue region represents the area where the fields were constrained to be attractive to the minority component to model the lower surface energy PDMS has with air as observed in experiment. T is the cell thickness and L_x and L_y are the post lattice dimensions.

References

1. Yang, J. K. W.; Jung, Y. S.; Chang, J.; Mickiewicz, R. A; Alexander-Katz, A.; Ross, C. A.; Berggren, K. K. Complex Self-Assembled Patterns Using Sparse Commensurate Templates with Locally Varying Motifs. ~~*Nature*~~ *Nat. Nanotechnol.* **2010**, 5, 256-260.

2. Mickiewicz, R. A.; Yang, J. K. W.; Hannon, A. F.; Jung, Y.; Alexander-Katz, A.; Berggren, K. K.; Ross, C. A. Enhancing the Potential of Block Copolymer Lithography with Polymer Self-Consistent Field Theory Simulations. *Macromolecules* **2010**, 43, 8290-8295.